Intermediate-valent $Ce_{23}Ru_7Mg_4$ and $RE_{23}Ru_7Mg_4$ (RE = La, Pr, Nd) with $Pr_{23}Ir_7Mg_4$-type Structure

Stefan Linsinger, Matthias Eul, Wilfried Hermes, Rolf-Dieter Hoffmann, and Rainer Pöttgen

Institut für Anorganische und Analytische Chemie, Universität Münster, Corrensstraße 30, 48149 Münster, Germany

Reprint requests to R. Pöttgen. E-mail: pottgen@uni-muenster.de

Z. Naturforsch. **2009**, *64b,* 1345 – 1352; received July 22, 2009

Dedicated to Professor Hubert Schmidbaur on the occasion of his 75th birthday

The rare earth-rich magnesium compounds $RE_{23}Ru_7Mg_4$ (RE = La, Ce, Pr, Nd) were synthesized from the elements in sealed tantalum ampoules in an induction furnace. They crystallize with the hexagonal non-centrosymmetric $Pr_{23}Ir_7Mg_4$-type structure, space group $P6_3mc$. The structures of $La_{23}Ru_{6.88(1)}Mg_4$ (a = 1017.7(4), c = 2286.5(5) pm, wR2 = 0.0277, 2708 F^2, 71 variables), $Ce_{23}Ru_7Mg_4$ (a = 993.5(3), c = 2243.9(8) pm, wR2 = 0.0573, 2268 F^2, 70 variables), and $Pr_{23}Ru_7Mg_4$ (a = 996.8(3), c = 2241.5(6) pm, wR2 = 0.0492, 2565 F^2, 70 variables) have been refined from single-crystal diffractometer data. The structures are built up from complex three-dimensional networks of edge- and corner-sharing RE_6Ru trigonal prisms. Cavities within these networks are filled by slightly elongated Mg_4 tetrahedra (311 – 315 pm in $Pr_{23}Ru_7Mg_4$) and RE_6 octahedra. The cerium compound has an a parameter which is even smaller than that of $Nd_{23}Ru_7Mg_4$, indicating intermediate-valent cerium. This was confirmed by magnetic susceptibility measurements. $Ce_{23}Ru_7Mg_4$ shows an average, reduced magnetic moment of 2.01 μ_B/Ce atom. $Pr_{23}Ru_7Mg_4$ contains stable trivalent praseodymium (3.64 μ_B/Pr atom).

Key words: Intermetallics, Cerium, Magnesium, Intermediate Valence

Introduction

The rare earth (RE)–transition metal (T)–magnesium systems have intensively been studied in recent years with respect to phase analyses, crystal structures, and chemical bonding as well as magnetic and mechanical properties. Such $RE_xT_yMg_z$ intermetallics have technical importance for precipitation hardening in modern light weight alloy systems [1]. Crystal chemical details have been reported in the literature [2 – 5, and references therein].

The RE-rich parts of the RE-T-Mg systems have intensively been investigated. Two new series of compounds with the compositions RE_4TMg (T = Co, Ni, Ru, Rh, Pd, Ir, Pt) [2, 6 – 8, and references therein] with Gd_4RhIn-type structure [9] and $RE_{23}T_7Mg_4$ (T = Ni, Rh, Ir) [10 – 12] with $Pr_{23}Ir_7Mg_4$-type [10] have been reported. Both structure types are closely related. The basic structural units are transition metal-centered trigonal prisms of the rare earth elements RE_6T which are condensed to complex three-dimensional networks. The latter is cubic for the Gd_4RhIn type (space group $F\bar{4}3m$) and hexagonal for the $Pr_{23}Ir_7Mg_4$ type (space group $P6_3mc$). Cavities within these networks are filled by tetrahedral Mg_4 clusters, a rare structural motif in magnesium chemistry [12].

Table 1. Lattice parameters (Guinier powder data) of the ternary magnesium compounds $RE_{23}Ru_7Mg_4$. The data marked with an asterisk refer to the investigated single crystals.

Compound	a (pm)	c (pm)	V (nm^3)
$La_{23}Ru_7Mg_4$	1017.7(4)	2286.5(5)	2.0510
$La_{23}Ru_{6.88(1)}Mg_4$*	1017.7(1)	2286.6(5)	2.0510
$Ce_{23}Ru_7Mg_4$	993.5(3)	2243.9(8)	1.9181
$Ce_{23}Ru_7Mg_4$*	993.5(1)	2243.9(5)	1.9181
$Pr_{23}Ru_7Mg_4$	996.8(3)	2241.5(6)	1.9288
$Pr_{23}Ru_7Mg_4$*	996.8(1)	2241.5(5)	1.9288
$Nd_{23}Ru_7Mg_4$	993.7(3)	2230.8(6)	1.9077

First investigations revealed interesting properties for these rare earth-rich materials. Gd_4NiMg exhibits antiferromagnetic ordering below T_N = 92 K [7]. It absorbs up to 11 hydrogen atoms per formula unit, leading to a drastic change of the magnetic properties. Gd_4NiMgH_{11} remains paramagnetic down to

Table 2. Crystal data and structure refinement for $RE_{23}Ru_7Mg_4$ (RE = La, Ce, Pr), space group $P6_3mc$, $Z = 2$.

Empirical formula	$La_{23}Ru_{6.88(1)}Mg_4$	$Ce_{23}Ru_7Mg_4$	$Pr_{23}Ru_7Mg_4$
Unit cell dimensions	Table 1	Table 1	Table 1
Molar mass, g mol^{-1}	3987.03	4027.49	4045.66
Calculated density, g cm^{-3}	6.46	6.97	6.97
Crystal size, μm^3	$20 \times 40 \times 40$	$30 \times 30 \times 80$	$30 \times 40 \times 80$
Transm. ratio (max/min)	2.17	1.81	1.78
Absorption coefficient, mm^{-1}	25.8	29.3	31.1
Detector distance, mm	80	90	80
Exposure time, min	3	3	3
ω range; increment, deg	0 – 180, 1.0	0 – 180, 1.0	0 – 180, 1.0
Integr. param. A, B, EMS	13.5; 3.0; 0.015	13.0; 3.0; 0.012	13.5; 3.5; 0.012
$F(000)$	3323	3380	3426
θ range for data collection, deg	2 – 32	2 – 31	2 – 32
Range in hkl	±15, ±15, ±34	±14, ±14, ±32	±14, ±14, ±33
Total no. reflections	25257	19214	43066
Independent reflections / R_{int}	2708 / 0.0551	2268 / 0.0543	2565 / 0.0887
Reflections with $I \geq 2\sigma(I)$ / R_σ	2178 / 0.0480	1429 / 0.0892	1760 / 0.0771
Data / parameters	2708 / 71	2268 / 70	2565 / 70
Goodness-of-fit on F^2	0.808	0.713	0.735
$R1$ / $wR2$ for $I \geq 2\sigma(I)$	0.0277 / 0.0253	0.0318 / 0.0543	0.0291 / 0.0467
$R1$ / $wR2$ for all data	0.0475 / 0.0277	0.0574 / 0.0573	0.0513 / 0.0492
Flack parameter	0.03(2)	0.02(5)	0.02(3)
Extinction coefficient	0.000143(4)	0.00022(1)	0.000224(9)
Largest diff. peak / hole, e Å^{-3}	1.95 / −2.17	3.81 / −1.75	1.85 / −1.90

2 K [7]. $Ce_{23}Ni_7Mg_4$ [11] and $Ce_{23}Rh_7Mg_4$ [12] are Curie-Weiss paramagnets with stable trivalent cerium. $Ce_{23}Rh_7Mg_4$ orders antiferromagnetically at 2.9 K. A highly interesting behavior was recently observed for the isotypic cadmium compounds $RE_{23}T_7Cd_4$ (T = Co, Ni, Ru, Rh, Ir, Pt) [13, 14]. All of these compounds fit well within the volume plots, indicating smooth behavior for the lanthanide contraction, except $Ce_{23}Ru_7Cd_4$ [13, 14]. Here, the a lattice parameter was even smaller than that of the praseodymium compound, and this peculiar behavior was rationalized with intermediate-valent cerium, similar to CeRuSn [15, 16], Ce_2RuZn_4 [17, 18], and CeRuAl [19]. Five of the nine crystallographically independent cerium sites in $Ce_{23}Ru_7Cd_4$ show Ce–Ru distances which are shorter than the Pr–Ru distances in $Pr_{23}Ru_7Cd_4$, indicating ordering of trivalent and intermediate-valent cerium in $Ce_{23}Ru_7Cd_4$. Keeping these interesting physical properties in mind, we were also interested in the corresponding magnesium compounds. Herein we report on the synthesis of the new compounds $RE_{23}Ru_7Mg_4$ with RE = La, Ce, Pr, Nd and their magnetic properties.

Experimental Section

Synthesis

Starting materials for the synthesis of the $RE_{23}Ru_7Mg_4$ samples were ingots of the rare earth metals (Johnson Matthey and smart elements, > 99.9 %), ruthenium powder (Heraeus, *ca.* 200 mesh, > 99.9 %), and a magnesium rod (Johnson Matthey, ∅ 16 mm, > 99.95 %, the surface layer of the rod was removed on a turning lathe). The rare earth metal ingots were first cut into smaller pieces and arc-melted [20] to small buttons under an argon atmosphere. The argon was purified with titanium sponge (900 K), silica gel, and molecular sieves.

The rare earth metal buttons, the ruthenium powder, and pieces of the magnesium rod were then weighed in the 23*RE*:7Ru:4Mg atomic ratios and arc-welded in tantalum tubes with about 1 cm^3 tube volume under an argon pressure of about 800 mbar. The ampoules were then placed in a water-cooled sample chamber [21] of a high-frequency furnace (Hüttinger Elektronik, Freiburg, Typ TIG 5/300) and heated for 2 min at about 1300 K, followed by 2 h at *ca.* 920 K. Finally the tubes were quenched to r. t. The $RE_{23}Ru_7Mg_4$ samples resulted as brittle reaction products. They could easily be separated from the tubes. No reaction with the container material was observed. Compact pieces and powders are stable in air. Powders are dark gray and single crystals exhibit metallic luster.

EDX data

Semiquantitative EDX analyses on the $RE_{23}Ru_7Mg_4$ crystals investigated on the diffractometer were carried out by use of a Leica 420i scanning electron microscope with LaF_3, CeO_2, PrF_3, Ru, and MgO as standards. The experimentally observed compositions were close to the ideal one. No impurity elements heavier than sodium (detection limit of the instrument) have been found.

X-Ray diffraction

All samples were characterized by Guinier diagrams (imaging plate detector, Fujifilm BAS-1800 readout system) with Cu$K\alpha_1$ radiation and α-quartz (a = 491.30 and c = 540.46 pm) as internal standard. The lattice parameters (Table 1) were refined by a least-squares routine. Accurate indexing was ensured through intensity calculations [22] taking the atomic positions from the structure refinements.

Small single crystals of $La_{23}Ru_7Mg_4$, $Ce_{23}Ru_7Mg_4$, and $Pr_{23}Ru_7Mg_4$ were selected from the crushed annealed samples. Their quality was checked by Laue photographs on a Buerger camera (white Mo radiation). Intensity data were collected at r.t. by use of a Stoe IPDS-II imaging plate diffractometer in oscillation mode (graphite-monochromatized MoK_α radiation). Numerical absorption corrections were applied to the data sets. All relevant details concerning the data collections and evaluations are listed in Table 2.

Structure refinements

The isotypy of the $RE_{23}Ru_7Mg_4$ compounds with the corresponding $RE_{23}T_7Mg_4$ compounds with T = Ni, Rh, Ir [10 – 12] could already be assumed from the Guinier patterns. Careful evaluation of the data sets then showed that the systematic extinctions were compatible with space group $P6_3mc$, in agreement with the $Pr_{23}Ir_7Mg_4$ type [10]. The atomic parameters of isotypic $La_{23}Rh_7Mg_4$ [12] were taken as starting values, and the three structures were refined using SHELXL-97 [23] (full-matrix least-squares on F^2) with anisotropic atomic displacement parameters for the rare earth and transition metal atoms and isotropic displacement parameters for the light magnesium atoms. Since the structure refinement of the prototype $Pr_{23}Ir_7Mg_4$ [10] revealed small defects on the Ir2 site, also the occupancy parameters of the $RE_{23}Ru_7Mg_4$ crystals were refined in separate series of least-squares cycles. Since for $Ce_{23}Ru_7Mg_4$ and $Pr_{23}Ru_7Mg_4$ all sites were fully occupied within two standard deviations, in the final cycles the ideal occupancy parameters were assumed again. In contrast, the $La_{23}Ru_7Mg_4$ crystal revealed small defects for the Ru2 site, and this occupancy parameter was refined as a least-squares variable in the final refinement, leading to a composition $La_{23}Ru_{6.88(1)}Mg_4$ for the investigated crystal. Refinement of the correct absolute structure was ensured through calculation of the Flack parameter [24, 25]. The final difference Fourier syntheses were flat (Table 2). The positional parameters and interatomic distances are listed in Tables 3 and 4.

Further details of the crystal structure investigations may be obtained from Fachinformationszentrum Karlsruhe, 76344 Eggenstein-Leopoldshafen, Germany (fax: +49-7247-808-666; e-mail: crysdata@fiz-karlsruhe.de, http://www.fiz-informationsdienste.de/en/DB/icsd/depot_anforderung.html) on quoting the deposition numbers CSD-420863 ($La_{23}Ru_7Mg_4$), CSD-420864 ($Ce_{23}Ru_7Mg_4$), and CSD-420865 ($Pr_{23}Ru_7Mg_4$).

Table 3. Atomic coordinates and isotropic displacement parameters (pm^2) for $La_{23}Ru_{6.88}Mg_4$, $Ce_{23}Ru_7Mg_4$ and $Pr_{23}Ru_7Mg_4$. U_{eq} is defined as one third of the trace of the orthogonalized U_{ij} tensor. The Ru2 site of $La_{23}Ru_{6.88(1)}Mg_4$ is occupied by 95.7(4) %. The investigated $La_{23}Ru_{6.88(1)}Mg_4$ single crystal had the other absolute structure.

Atom	W. position	x	y	z	U_{eq}
$La_{23}Ru_{6.88(1)}Mg_4$					
La1	6*c*	0.87229(4)	$-x$	0.86461(3)	137(1)
La2	6*c*	0.79238(4)	$-x$	0.71840(2)	121(1)
La3	6*c*	0.79179(4)	$-x$	0.55040(2)	125(1)
La4	6*c*	0.79172(5)	$-x$	0.00780(3)	181(1)
La5	6*c*	0.45894(4)	$-x$	0.91372(5)	128(1)
La6	6*c*	0.45990(4)	$-x$	0.64381(2)	158(1)
La7	2*b*	2/3	1/3	0.85320(4)	114(2)
La8	2*a*	0	0	0.99784(5)	125(2)
La9	6*c*	0.20781(4)	$-x$	0.78032(3)	131(1)
Ru1	6*c*	0.51676(5)	$-x$	0.78916(3)	167(2)
Ru2	6*c*	0.14692(5)	$-x$	0.93819(4)	178(3)
Ru3	2*b*	2/3	1/3	0.62957(6)	174(3)
Mg1[a]	6*c*	0.10373(19)	$-x$	0.63609(17)	145(7)
Mg2[a]	2*a*	0	0	0.7480(2)	135(13)
$Ce_{23}Ru_7Mg_4$					
Ce1	6*c*	0.12924(7)	$-x$	0.13586(5)	153(2)
Ce2	6*c*	0.20521(8)	$-x$	0.28324(5)	154(2)
Ce3	6*c*	0.20824(8)	$-x$	0.44962(5)	144(3)
Ce4	6*c*	0.20888(10)	$-x$	0.99330(6)	234(3)
Ce5	6*c*	0.54097(7)	$-x$	0.08446(6)	139(2)
Ce6	6*c*	0.54028(8)	$-x$	0.35721(5)	174(3)
Ce7	2*b*	1/3	2/3	0.14645(9)	150(4)
Ce8	2*a*	0	0	0.99880(10)	158(4)
Ce9	6*c*	0.79154(7)	$-x$	0.21967(7)	149(2)
Ru1	6*c*	0.48599(12)	$-x$	0.21213(9)	361(5)
Ru2	6*c*	0.85134(12)	$-x$	0.05670(12)	421(6)
Ru3	2*b*	1/3	2/3	0.37306(17)	349(9)
Mg1[a]	6*c*	0.8949(3)	$-x$	0.3643(3)	113(13)
Mg2[a]	2*a*	0	0	0.2495(5)	82(23)
$Pr_{23}Ru_7Cd_4$					
Pr1	6*c*	0.12820(5)	$-x$	0.13608(4)	114(2)
Pr2	6*c*	0.20741(6)	$-x$	0.28182(3)	99(2)
Pr3	6*c*	0.20817(6)	$-x$	0.44937(3)	107(2)
Pr4	6*c*	0.20890(7)	$-x$	0.99301(4)	162(2)
Pr5	6*c*	0.54117(6)	$-x$	0.08535(4)	102(2)
Pr6	6*c*	0.54065(6)	$-x$	0.35661(5)	136(2)
Pr7	2*b*	1/3	2/3	0.14611(6)	92(3)
Pr8	2*a*	0	0	0.00211(7)	105(3)
Pr9	6*c*	0.79168(5)	$-x$	0.21951(5)	108(2)
Ru1	6*c*	0.48280(8)	$-x$	0.21015(5)	155(3)
Ru2	6*c*	0.85346(8)	$-x$	0.06237(6)	182(3)
Ru3	2*b*	1/3	2/3	0.36935(11)	176(5)
Mg1[a]	6*c*	0.8947(3)	$-x$	0.3640(3)	111(11)
Mg2[a]	2*a*	0	0	0.2514(4)	75(18)

[a] These positions have been refined with isotropic displacement parameters.

Table 4. Interatomic distances (pm) of $La_{23}Ru_{6.88(1)}Mg_4$, $Ce_{23}Ru_7Mg_4$ and $Pr_{23}Ru_7Mg_4$, calculated with the powder lattice parameters. Standard deviations are all equal or smaller than 0.9 pm.

$La_{23}Ru_{6.88(1)}Mg_4$				**$Ce_{23}Ru_7Mg_4$**				**$Pr_{23}Ru_7Mg_4$**			
La1:	2	Ru2	296.2	Ce1:	2	Ru2	299.3	Pr1:	2	Ru2	290.4
	1	Mg2	348.9		1	Mg2	338.3		1	Mg2	340.3
	1	La4	356.9		1	Ce4	348.0		1	Pr4	349.7
	1	La2	362.8		1	Ce7	352.0		1	Pr2	354.1
	1	La7	363.4		1	Ce2	355.6		1	Pr7	354.9
	2	Ru1	367.7		2	Ru1	359.7		2	Ru1	358.0
	2	La9	373.6		2	Ce9	365.7		2	Pr9	365.7
	1	La8	378.8		2	Ce5	372.6		1	Pr8	373.1
	2	La5	381.2		1	Ce8	379.5		2	Pr5	374.2
	2	La1	389.9		2	Ce1	385.2		2	Pr1	383.4
La2:	2	Ru1	294.2	Ce2:	2	Ru1	291.8	Pr2:	2	Ru1	289.1
	1	Ru3	300.6		1	Ru3	298.7		1	Ru3	292.9
	2	La6	360.9		2	Ce6	352.8		1	Pr1	354.1
	1	La1	362.8		1	Ce1	355.6		2	Pr6	354.5
	2	Mg1	368.6		2	Mg1	355.9		2	Mg1	360.7
	1	Mg2	372.2		1	Mg2	361.2		1	Mg2	364.5
	1	La7	379.6		1	Ce3	373.4		1	Pr7	373.9
	2	La2	383.8		1	Ce7	377.9		1	Pr3	375.6
	1	La3	384.1		2	Ce2	381.9		2	Pr2	376.6
	2	La9	392.6		2	Ce9	383.5		2	Pr9	385.1
La3:	1	Ru2	278.4	Ce3:	1	Ru2	261.2	Pr3:	1	Ru2	274.7
	1	Ru3	285.3		1	Ru3	275.4		1	Ru3	280.8
	2	Mg1	373.4		2	Mg1	364.6		2	Mg1	365.4
	2	La4	379.8		2	Ce5	371.6		2	Pr4	373.1
	2	La3	382.0		2	Ce4	372.0		2	Pr5	373.8
	2	La5	382.8		2	Ce3	372.9		2	Pr3	374.3
	2	La6	383.0		1	Ce2	373.4		2	Pr6	375.1
	1	La2	384.1		2	Ce6	373.5		1	Pr2	375.6
	1	La8	386.2		1	Ce8	374.9		1	Pr8	378.3
La4:	1	Mg1	346.4	Ce4:	1	Mg1	340.0	Pr4:	1	Mg1	340.0
	1	La1	356.9		1	Ce1	348.0		1	Pr1	349.7
	2	Ru2	363.5		2	Ru2	350.6		2	Ru2	356.4
	1	La8	367.8		1	Ce8	359.7		1	Pr8	361.2
	2	La3	379.8		2	Ce4	370.9		2	Pr4	372.1
	2	La4	381.8		2	Ce3	372.0		2	Pr3	373.1
	2	La6	382.0		2	Ce5	372.6		2	Pr6	374.5
	2	La5	385.0		2	Ce6	374.0		2	Pr5	375.1
	1	La7	416.6		1	Ce7	404.9		1	Pr7	404.9
La5:	2	Ru2	295.6	Ce5:	2	Ru2	288.0	Pr5:	2	Ru2	289.4
	1	Ru1	302.5		1	Ru1	301.7		1	Ru1	297.4
	2	La9	376.9		2	Ce3	371.6		2	Pr9	370.4
	2	La1	381.2		2	Ce9	372.2		2	Pr3	373.8
	2	La3	382.7		2	Ce1	372.6		2	Pr1	374.2
	2	La5	383.5		2	Ce4	372.6		2	Pr4	375.0
	2	La4	385.0		2	Ce5	374.6		2	Pr5	375.3
	1	La7	391.4		1	Ce7	383.4		1	Pr7	383.8

Table 4 (continued).

$La_{23}Ru_{6.88(1)}Mg_4$				**$Ce_{23}Ru_7Mg_4$**				**$Pr_{23}Ru_7Mg_4$**			
La6:	1	Ru1	347.1	Ce6:	1	Ru1	338.7	Pr6:	2	Mg1	342.0
	2	Mg1	351.6		2	Mg1	341.1		1	Ru1	343.2
	2	La2	360.9		2	Ce2	352.8		2	Pr2	354.5
	1	Ru3	365.9		1	Ru3	357.9		1	Ru3	359.1
	2	La4	382.0		2	Ce3	373.5		2	Pr4	374.5
	2	La3	383.0		2	Ce4	374.0		2	Pr3	375.1
	2	La9	383.1		2	Ce6	376.7		2	Pr9	376.0
	2	La6	386.4		2	Ce9	376.8		2	Pr6	376.8
La7:	3	Ru1	302.1	Ce7:	3	Ru1	301.2	Pr7:	3	Ru1	295.3
	3	La1	363.4		3	Ce1	352.0		3	Pr1	354.9
	3	La2	379.6		3	Ce2	377.9		3	Pr2	373.9
	3	La5	391.4		3	Ce5	383.4		3	Pr5	383.8
	3	La4	416.6		3	Ce4	404.9		3	Pr4	404.9
La8:	3	Ru2	292.7	Ce8:	3	Ru2	286.9	Pr8:	3	Ru2	286.8
	3	Mg1	365.2		3	Mg1	351.9		3	Mg1	359.0
	3	La4	367.8		3	Ce4	359.7		3	Pr4	361.2
	3	La1	378.9		3	Ce3	374.9		3	Pr1	373.1
	3	La3	386.2		3	Ce1	379.5		3	Pr3	378.4
La9:	2	Ru1	287.0	Ce9:	2	Ru1	276.3	Pr9:	2	Ru1	281.6
	2	La1	373.6		1	Mg2	364.9		2	Pr1	365.7
	1	Mg2	373.7		2	Ce1	365.7		1	Mg2	366.7
	1	Ru2	376.6		1	Mg1	370.1		1	Ru2	368.1
	2	La5	376.9		2	Ce9	372.2		1	Mg1	369.5
	1	Mg1	377.4		2	Ce5	372.2		2	Pr5	370.4
	2	La6	383.1		2	Ce6	376.8		2	Pr9	373.9
	2	La9	383.2		1	Ru2	379.9		2	Pr6	376.0
	2	La2	392.6		2	Ce2	383.5		2	Pr2	385.1
Ru1:	2	La9	287.0	Ru1:	2	Ce9	276.3	Ru1:	2	Pr9	281.6
	2	La2	294.2		2	Ce2	291.8		2	Pr2	289.1
	1	La7	302.1		1	Ce7	301.2		1	Pr7	295.3
	1	La5	302.5		1	Ce5	301.7		1	Pr5	297.4
	1	La6	347.1		1	Ce6	338.7		1	Pr6	343.2
	2	La1	367.7		2	Ce1	359.7		2	Pr1	358.0
Ru2:	1	La3	278.4	Ru2:	1	Ce3	261.2	Ru2:	1	Pr3	274.7
	1	La8	292.7		1	Ce8	286.9		1	Pr8	286.8
	2	La5	295.6		2	Ce5	288.0		2	Pr5	289.4
	2	La1	296.2		2	Ce1	299.3		2	Pr1	290.4
	2	La4	363.5		2	Ce4	350.6		2	Pr4	356.4
	1	La9	376.6		1	Ce9	379.9		1	Pr9	368.1
Ru3:	3	La3	285.3	Ru3:	3	Ce3	275.4	Ru3:	3	Pr3	280.8
	3	La2	300.6		3	Ce2	298.7		3	Pr2	292.9
	3	La6	365.9		3	Ce6	357.9		3	Pr6	359.1
Mg1:	1	Mg2	314.5	Mg1:	2	Mg1	313.4	Mg1:	1	Mg2	311.1
	2	Mg1	316.7		1	Mg2	314.9		2	Mg1	314.9
	1	La4	346.4		1	Ce4	340.1		1	Pr4	340.0
	2	La6	351.6		2	Ce6	341.1		2	Pr6	342.0
	1	La8	365.2		1	Ce8	351.9		1	Pr8	359.0
	2	La2	368.6		2	Ce2	355.9		2	Pr2	360.7
	2	La3	373.4		2	Ce3	364.6		2	Pr3	365.4
	1	La9	377.4		1	Ce9	370.1		1	Pr9	369.5
Mg2:	3	Mg1	314.5	Mg2:	3	Mg1	314.9	Mg2:	3	Mg1	311.1
	3	La1	348.9		3	Ce1	338.3		3	Pr1	340.2
	3	La2	372.2		3	Ce2	361.2		3	Pr2	364.5
	3	La9	373.7		3	Ce9	364.9		3	Pr9	366.7

Physical property measurements

The magnetic and heat capacity measurements were carried out on a Quantum Design Physical Property Measurement System (PPMS) using the VSM and heat capacity options, respectively. For VSM measurements, the samples (15.135 mg for $Ce_{23}Ru_7Mg_4$; 27.311 mg for $Pr_{23}Ru_7Mg_4$) were packed in kapton foil and attached to the sample holder rod for measuring the magnetic properties in the temperature range 2.2 – 305 K with magnetic flux densities up to 80 kOe. For heat capacity (C_P) measurements (2.1 – 300 K)

the samples (7.265 mg for $Ce_{23}Ru_7Mg_4$; 26.024 mg for $Pr_{23}Ru_7Mg_4$) were fixed to the platform of a pre-calibrated heat capacity puck using Apiezon N grease.

Discussion

Crystal chemistry

The ternary rare earth-rich compounds $RE_{23}Ru_7Mg_4$ with *RE* = La, Ce, Pr, Nd are new members of the family of compounds with the complex hexagonal $Pr_{23}Ir_7Mg_4$ type [10]. Similar to the other isotypic series $RE_{23}T_7Mg_4$ (*T* = Ni, Rh, Ir) [10–12] and $RE_{23}T_7Cd_4$ (*T* = Co, Ni, Ru, Rh, Ir, Pt) [13, 14]), also the $RE_{23}Ru_7Mg_4$ compounds only form with the larger rare earth elements. With the smaller rare earth elements only the RE_4TMg [2, 6–8] and RE_4TCd [26] phases exist. Since the crystal chemistry of the RE_4TMg and $RE_{23}T_7Mg_4$ phases has repeatedly been discussed, herein we focus only on the structural peculiarities within the $RE_{23}Ru_7Mg_4$ series.

As is evident from Table 1, the lattice parameter *a* of $Ce_{23}Ru_7Mg_4$ is even smaller than the one of $Nd_{23}Ru_7Mg_4$, while the lattice parameter *c* of $Ce_{23}Ru_7Mg_4$ is compatible with the lanthanide contraction. This result is very similar to the $RE_{23}Ru_7Cd_4$ series [13, 14]. Due to the intermediate-valent character of some of the cerium atoms in $Ce_{23}Ru_7Mg_4$ (*vide infra*), one observes shorter Ce–Ru distances for those. Since the Ce_6Ru trigonal prisms as the main building blocks in $Ce_{23}Ru_7Mg_4$ are predominantly condensed in the *ab* direction (Fig. 1), this shortening of the Ce–Ru distances expresses itself also in a significant contraction of the *a* direction.

In order to see the influence of the intermediate cerium valence on the local ruthenium coordination, we have refined the structure of $Ce_{23}Ru_7Mg_4$ and also those with the neighboring rare earth elements, *i. e.* $La_{23}Ru_7Mg_4$ and $Pr_{23}Ru_7Mg_4$ from single-crystal X-ray data. The interatomic distances are listed in Table 4, and the different ruthenium coordination polyhedra (tricapped trigonal prisms) are presented in Fig. 2.

Within the tricapped trigonal prisms, each ruthenium atom has six closer cerium neighbors building the prisms, while the three cerium atoms caping the latter are at somewhat longer distances. This way we can describe the near-neighbor environment as a typical 6 + 3 coordination. The Ce–Ru distances for the six closest neighbors range from 261 to 302 pm. Several of these Ce–Ru distances are smaller than the sum of

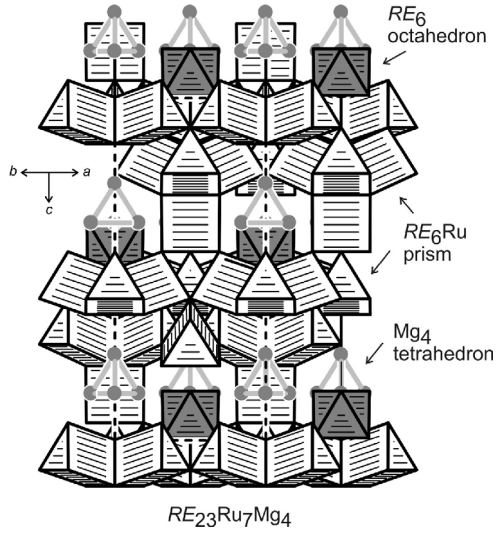

Fig. 1. View of the $RE_{23}Ru_7Mg_4$ structure approximately along the [110] direction. The network of condensed trigonal $RuRE_6$ prisms, the Mg_4 tetrahedra and the empty RE_6 octahedra (medium gray shading) are emphasized.

the covalent radii [27] of 289 pm for cerium and ruthenium. Such short Ce–Ru distances are a strong hint for intermediate-valent (*i. e.* smaller) cerium. In the meantime, such short Ce–Ru distances have repeatedly been observed for binary and ternary cerium intermetallics. A full list has been published recently [19]. Electronic structure calculations for CeRuSn [16], Ce_2RuZn_4 [18], and CeRuAl [19] showed strong Ce–Ru bonding for these interactions.

Finally we compare the $RE_{23}Ru_7Mg_4$ (*RE* = La, Ce, Pr) series with the isotypic $RE_{23}Ru_7Cd_4$ (*RE* = La, Ce, Pr) compounds [13, 14]. Although cadmium (141 pm) has a larger covalent radius [27] than magnesium (136 pm), the course of the lattice parameters for $Ce_{23}Ru_7Mg_4$ (a = 993.5(3) and c = 2243.9(8) pm, V = 1.9181 nm^3) and $Ce_{23}Ru_7Cd_4$ [13, 14] (a = 988.7(3), c = 2241.6(5) pm, V = 1.8977 nm^3) shows the inverse trend. This already indicates a stronger trend *versus* intermediate-valent cerium in the cadmium compound, in agreement with the course of the Pauling electronegativities of 1.31 for magnesium and 1.69 for cadmium [27].

These trends are in line with small differences in the cerium near neighbor coordinations of $Ce_{23}Ru_7Mg_4$ and $Ce_{23}Ru_7Cd_4$. In the structure of the cadmium compound (the same setting has been used for both structure refinements), the Ce1, Ce2, Ce5, and Ce7 atoms can be considered as purely trivalent, while Ce3, Ce4,

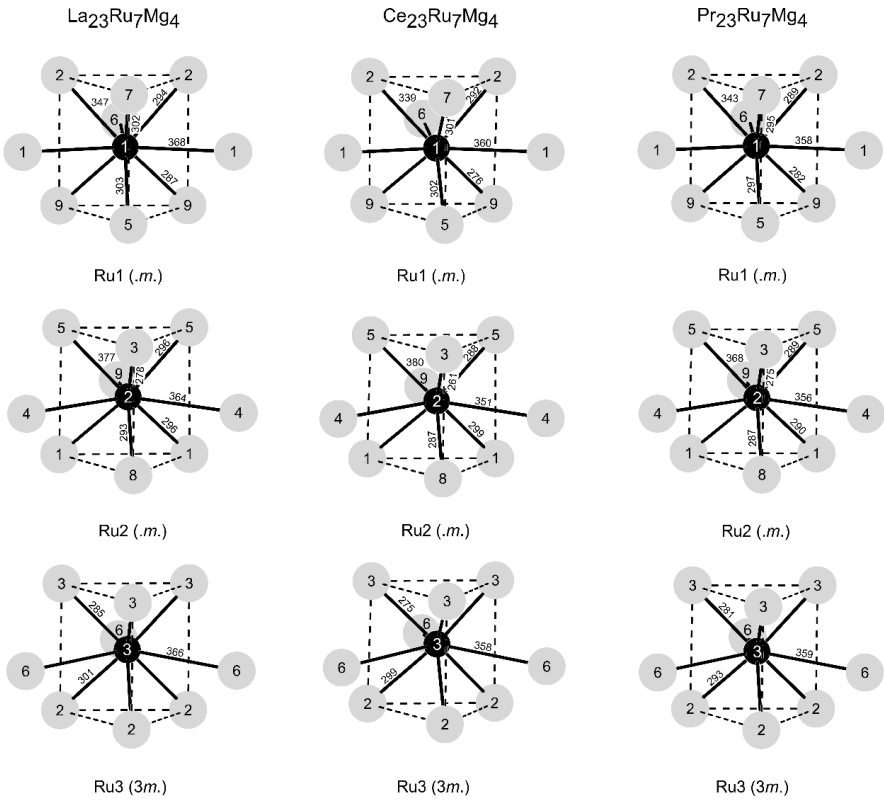

Fig. 2. Near-neighbor coordination of the ruthenium atoms in $RE_{23}Ru_7Mg_4$ (*RE* = La, Ce, Pr). Rare earth and ruthenium atoms are drawn as light gray and black circles, respectively. Relevant interatomic distances are indicated.

Ce6, Ce8, and Ce9 are in an intermediate valence state. This is slightly different in $Ce_{23}Ru_7Mg_4$. Here, Ce1, Ce2, Ce7, and Ce8 can be considered as trivalent (larger Ce–Ru than Pr–Ru distances), while Ce3, Ce4, Ce5, Ce6, and Ce9 tend towards intermediate cerium valence. Thus, 30 of the 46 cerium atoms per unit cell are in an intermediate valence state. The differences between the $Ce_{23}Ru_7Mg_4$ and $Ce_{23}Ru_7Cd_4$ structures are due to the difference in size of the Mg_4 and Cd_4 tetrahedra which slightly influences the cerium coordinations also.

The resulting experimental magnetic moment of $Ce_{23}Ru_7Mg_4$ in the paramagnetic regime (*vide infra*) is the average of the nine crystallographically independent cerium atoms. An assignment of the degree of intervalency based on these data is not possible. As a consequence of the intermediate cerium valence, the ruthenium atoms show enhanced displacements (Table 3) as compared to $Pr_{23}Ru_7Mg_4$ and $Nd_{23}Ru_7Mg_4$.

Physical properties

In Fig. 3 the temperature dependence of the inverse magnetic susceptibility of $Ce_{23}Ru_7Mg_4$ and

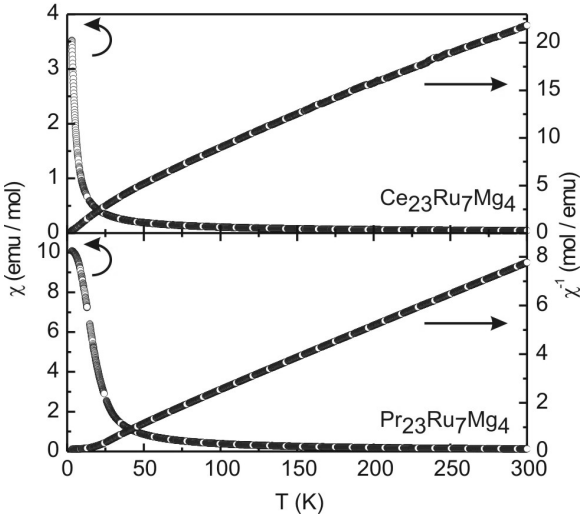

Fig. 3. Temperature dependence of the magnetic susceptibility (χ and χ^{-1} data) of $Ce_{23}Ru_7Mg_4$ and $Pr_{23}Ru_7Mg_4$ measured at 10 kOe.

$Pr_{23}Ru_7Mg_4$ is shown. The reciprocal magnetic susceptibility of $Ce_{23}Ru_7Mg_4$ had to be fitted with a modified Curie-Weiss law $\chi^{-1} = [\chi_0 + (C/T - \theta_P)]^{-1}$

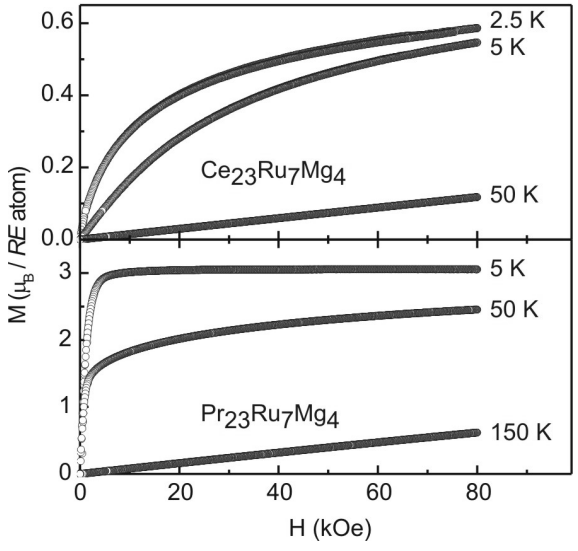

Fig. 4. Magnetization isotherms of $Ce_{23}Ru_7Mg_4$ and $Pr_{23}Ru_7Mg_4$ measured at various temperatures.

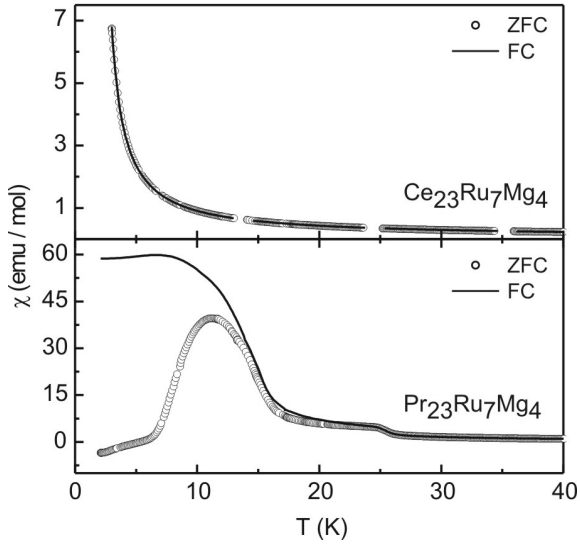

Fig. 5. Low-temperature susceptibility measurements (zero field cooled and field cooled states) of $Ce_{23}Ru_7Mg_4$ and $Pr_{23}Ru_7Mg_4$ measured at 100 Oe.

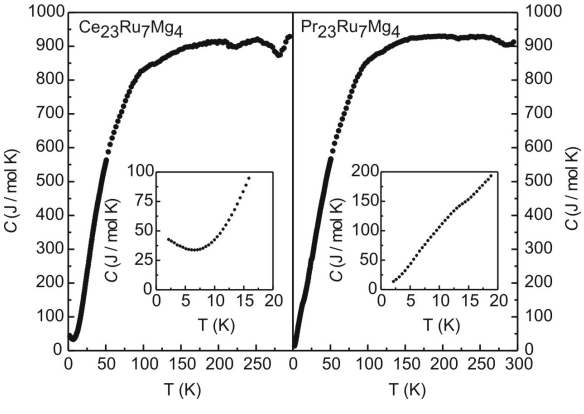

Fig. 6. Heat capacity measurements of $Ce_{23}Ru_7Mg_4$ and $Pr_{23}Ru_7Mg_4$ without an external applied field. The insets magnify the low-temperature range up to 20 K.

above 50 K, leading to a temperature-independent term $\chi_0 = 8.7(3) \times 10^{-3}$ emu mol^{-1}, a Weiss constant of $\theta_P = -13.7(8)$ K and an effective paramagnetic moment of $\mu_{eff} = (8C/23)^{1/2} = 2.01(3)$ μ_B per Ce atom. This value is significantly lower than the free ion value of 2.54 μ_B for Ce^{3+} and can be attributed to not all cerium atoms being in a trivalent state. The effective moment is equal to about 63 % of Ce^{3+} in the compound and is in accordance with the crystal data (*vide supra*). Due to the nine crystallographically independent cerium sites with different site symmetries, we are not able to assign the oxidation state for each site. The negative Weiss constant is indicative of antiferromagnetic interactions, though no magnetic ordering was detected down to 3 K. In contrast we observe a Curie-Weiss behavior for $Pr_{23}Ru_7Mg_4$ above 50 K with an experimental effective magnetic moment of 3.64(1) μ_B per Pr atom which is in good agreement with the free ion value of 3.58 μ_B for Pr^{3+}. Extrapolation of the χ^{-1} *vs.* T data to $\chi^{-1} = 0$ led to a Weiss constant of $\theta_P = 2.4(2)$ K for $Pr_{23}Ru_7Mg_4$, indicative of ferromagnetic interactions. No magnetic ordering down to 3 K was detected for the praseodymium compound.

The magnetization isotherms taken at 2.5, 5, and 50 K for $Ce_{23}Ru_7Mg_4$ as well as those taken at 5, 50, and 150 K for $Pr_{23}Ru_7Mg_4$ are displayed in Fig. 4. We observe an almost linear increase of the magnetization with the applied field at 50 K for the $Ce_{23}Ru_7Mg_4$ and at 25 K for the corresponding praseodymium compound as expected for a paramagnetic material. At 2.5 and 5 K the curvatures of the magnetization isotherms of $Ce_{23}Ru_7Mg_4$ become more pronounced and show a tendency for saturation at high fields. It may be noted here that the maximum saturation moment of 0.59(1) μ_B per Ce atom observed at 80 kOe and 2.5 K does not reach the expected moment value of 2.14 μ_B per Ce atom (according to $g_J \times J$). The reduced moment can be ascribed to crystal field splitting of the $J = 5/2$ ground state and due to the fact that not all Ce atoms are in a

stable trivalent state. This has also been observed in $Ce_{23}Ru_7Cd_4$ [14].

At 5 K the magnetization isotherm of $Pr_{23}Ru_7Mg_4$ is indicative of parallelly oriented magnetic moments, with no hysteresis being noted. The saturation magnetization at 80 kOe and 5 K is 3.05(1) μ_B per Pr atom, which is in a good agreement with the theoretical value of 3.20 μ_B per Pr atom, indicating full parallel spin alignment.

The low-field susceptibility (H = 100 Oe) measured in the zero field cooled (ZFC) and field cooled (FC) states of the samples is represented in Fig. 5. For $Ce_{23}Ru_7Mg_4$ no magnetic ordering could be observed down to 2.2 K. However, kink-point measurements display ferro- or ferrimagnetic ordering for $Pr_{23}Ru_7Mg_4$ at around 15 K. Below this temperature a strong bifurcation between the ZFC and FC states is clearly visible. At 25 K there is an additional small anomaly visible (not seen in heat capacity), which can be attributed to minor impurities of Pr_3Ru ordering ferromagnetically (T_C = 25 K [28]). Due to the absence of a λ-like anomaly and only a broad peak in the heat capacity measurement at around 15 K (see inset of Fig. 6) in $Pr_{23}Ru_7Mg_4$, long-range magnetic ordering can be ruled out. These findings in conjunction with the strong bifurcation observed in ZFC-FC measurement below 13 K, are indicative of a spin glass behavior without long-range magnetic ordering. The heat capacity measurement of $Ce_{23}Ru_7Mg_4$ shows an upturn starting at around 6 K (see inset of Fig. 6). This fact, in conjunction with the steep upturn in the ZFC-FC measurement, suggests the onset of long-range ferro- or ferrimagnetic ordering.

Acknowledgements

We are indebted to Dipl.-Ing. U. Ch. Rodewald for the intensity data collections. This work was financially supported by the Deutsche Forschungsgemeinschaft. W. H. thanks the NRW Graduate School of Chemistry and the Fonds der Chemischen Industrie for a PhD stipend.

[1] K. U. Kainer (Ed.), *Magnesium, Proceedings of the 6th International Conference on Magnesium Alloys and their Applications*, Wiley-VCH, Weinheim, **2004**.
[2] U. Ch. Rodewald, B. Chevalier, R. Pöttgen, *J. Solid State Chem.* **2007**, *180*, 1720.
[3] P. Solokha, S. De Negri, A. Saccone, V. Pavlyuk, B. Marciniak, J.-C. Tedenac, *Acta Crystallogr.* **2007**, *C63*, i13.
[4] S. De Negri, P. Solokha, A. Saccone, V. Pavlyuk, *Intermetallics* **2009**, *17*, 614.
[5] P. Solokha, S. De Negri, V. Pavlyuk, A. Saccone, *Solid State Sci.* **2009**, *11*, 801.
[6] S. Tuncel, B. Chevalier, R. Pöttgen, *Z. Naturforsch.* **2008**, *63b*, 600.
[7] S. Tuncel, J. G. Roquefère, C. Stan, J.-L. Bobet, B. Chevalier, E. Gaudin, R.-D. Hoffmann, U. Ch. Rodewald, R. Pöttgen, *J. Solid State Chem.* **2009**, *182*, 229.
[8] S. Linsinger, W. Hermes, B. Chevalier, S. Couillaud, J.-L. Bobet, M. Eul, R. Pöttgen, *Intermetallics* **2009**, *17*, 1028.
[9] R. Zaremba, U. Ch. Rodewald, R.-D. Hoffmann, R. Pöttgen, *Monatsh. Chem.* **2007**, *138*, 523.
[10] U. Ch. Rodewald, S. Tuncel, B. Chevalier, R. Pöttgen, *Z. Anorg. Allg. Chem.* **2008**, *634*, 1011.
[11] S. Tuncel, W. Hermes, B. Chevalier, U. Ch. Rodewald, R. Pöttgen, *Z. Anorg. Allg. Chem.* **2008**, *634*, 2140.
[12] S. Linsinger, S. Tuncel, W. Hermes, M. Eul, B. Chevalier, R. Pöttgen, *Z. Anorg. Allg. Chem.* **2009**, *635*, 282.
[13] F. Tappe, R. Pöttgen, *Z. Naturforsch.* **2009**, *64b*, 184.
[14] F. Tappe, W. Hermes, M. Eul, R. Pöttgen, *Intermetallics* **2009**, *17*, 1035.
[15] J. F. Riecken, W. Hermes, B. Chevalier, R.-D. Hoffmann, F. M. Schappacher, R. Pöttgen, *Z. Anorg. Allg. Chem.* **2007**, *633*, 1094.
[16] S. F. Matar, J. F. Riecken, B. Chevalier, R. Pöttgen, V. Eyert, *Phys. Rev. B* **2007**, *76*, 174434.
[17] R. Mishra, W. Hermes, U. Ch. Rodewald, R.-D. Hoffmann, R. Pöttgen, *Z. Anorg. Allg. Chem.* **2008**, *634*, 470.
[18] V. Eyert, E.-W. Scheidt, W. Scherer, W. Hermes, R. Pöttgen, *Phys. Rev. B* **2008**, *78*, 214420.
[19] W. Hermes, S. F. Matar, R. Pöttgen, *Z. Naturforsch.* **2009**, *64b*, 901.
[20] R. Pöttgen, Th. Gulden, A. Simon, *GIT Labor-Fachzeitschrift* **1999**, *43*, 133.
[21] D. Kußmann, R.-D. Hoffmann, R. Pöttgen, *Z. Anorg. Allg. Chem.* **1998**, *624*, 1727.
[22] K. Yvon, W. Jeitschko, E. Parthé, *J. Appl. Crystallogr.* **1977**, *10*, 73.
[23] G. M. Sheldrick, SHELXL-97, Program for Crystal Structure Refinement, University of Göttingen, (Göttingen) Germany **1997**. See also: G. M. Sheldrick, *Acta Crystallogr.* **2008**, *A64*, 112.
[24] H. D. Flack, G. Bernadinelli, *Acta Crystallogr.* **1999**, *A55*, 908.
[25] H. D. Flack, G. Bernadinelli, *J. Appl. Crystallogr.* **2000**, *33*, 1143.
[26] F. M. Schappacher, R. Pöttgen, *Monatsh. Chem.* **2008**, *139*, 1137.
[27] J. Emsley, *The Elements*, Oxford University Press, Oxford **1999**.
[28] C. S. Garde, J. Ray, *J. Magn. Magn. Mater.* **1998**, *189*, 293.